

On the Failure of Round-Hole Tubes under Cyclic Bending

Kuo-Long Lee*, Mu-Li Weng** and Wen-Fung Pan***

Keywords : round-hole tubes, cyclic bending, failure, finite element analysis.

ABSTRACT

This paper presents an experiment and an analysis for examining the response and failure of round-hole 6061-T6 aluminum alloy tubes with different hole diameters and hole directions subjected to cyclic bending. The moment-curvature response demonstrated an almost stable and closed hysteresis loop from the first bending cycle. The hole diameters and directions had almost no influence on the loop configuration. However, the ovalization-curvature behavior depicted an asymmetrical, ratcheting, and bow trend with the increase in the number of bending cycles, while hole diameters and directions exhibited a strong influence on this relationship. Finally, the finite-element software ANSYS was employed to describe the moment-curvature and ovalization-curvature relationships, and an empirical model was proposed to simulate the relationship between the controlled curvature and the number of bending cycles required to ignite failure. As a result, the experimental and analytical data were found to agree well.

INTRODUCTION

A round-hole tube is a tube with a circular hole drilled through. Round-hole tubes are often used as connections in parts of cars, locomotives, or bicycles. When a round-hole tube is subjected to a bending load, the circular cross section will gradually change to an elliptical shape with the increase of the bending. This will cause the bending rigidity of the tube to gradually decrease, which is called the degradation

phenomenon. To quantify the degradation phenomenon, a physical quantity called ovalization is employed, which is the reduction of the outer diameter ($\Delta D_o = D_o - D$) divided by the original outer diameter (D_o). In cyclic bending loads, the ovalization increases with the number of bending cycles. Finally, when a certain number of bending cycles is reached and the ovalization reaches a certain critical value, the round-hole tube will undergo fracture failure.

As part of the earlier study on this topic, Kyriakides' research team experimentally and theoretically investigated the response and collapse of tubes subjected to bending with or without internal or external pressure. Kyriakides and Shaw (1987) examined the stability of tubes under cyclic bending and an empirical model was introduced to simulate the cyclic controlled curvature (κ_c)-the number of cycles required to ignite buckling (N_b) relationship. Later, Corona and Kyriakides (1991) experimentally studied the deterioration and collapse of tubes submitted to cyclic bending with some external pressure. Thereafter, Vaze and Corona (1998) experimentally investigated the deterioration and stability of square cross-sectional steel tubes under cyclic bending and discovered that the tubes deteriorated as periodic and transverse displacements increased in the flange. In 2000, Corona and Kyriakides (2000) studied the tube's collapse under bending with some external pressure. Later, Corona et al. (2006) found that the tubes exhibited the plastic anisotropy. Moreover, they used Hill's yield function to measure and characterize this anisotropy. Thereafter, Limam et al. (2010) experimentally and analytically investigated the inelastic response and collapse of tubes under internal pressure and Limam et al. (2012) studied the influence of local dents on the collapse curvature of tubes under pure bending with some internal pressure. Bechle and Kyriakides (2014) later studied the localization of NiTi tubes submitted to bending. In addition, the influence of the texture-driven and complex material asymmetry on a simple structure were also investigated. Later, Jiang et al. (2017) implemented a constitutive model in a finite element analysis for simulating the pseudoelastic behavior of NiTi tubes subjected to bending.

Paper Received February, 2019. Revised July, 2019, Accepted August, 2019, Author for Correspondence: Wen-Fung Pan.

**Professor, Department of Innovative Design and Entrepreneurship Management, Far East University, Tainan, Taiwan 744, ROC.*

***Graduate Student, Department of Engineering Science, National Cheng Kung University, Tainan, Taiwan 701, ROC.*

****Professor, Department of Engineering Science, National Cheng Kung University, Tainan, Taiwan 701, ROC.*

Several researchers have also published related studies. Yuan and Mirmiran (2001) investigated the buckling of concrete-filled fiber-reinforced plastic tubes submitted to bending. Elchalakani et al. (2002) conducted tests on grade C350 steel tubes with different diameter-to-thickness ratios (D_o/t ratios) under bending. Jiao and Zhao (2004) experimentally studied the behavior of very-high-strength steel tubes submitted to bending. Corradi et al. (2005) examined the sensitivity of imperfection for circular tubes under external pressure. Elchalakani et al. (2006) determined the ductile section slenderness limits for the cold-formed CHS by conducting cyclic bending tests. Elchalakani and Zhao (2008) investigated the response for concrete-filled cold-formed steel tubes submitted to cyclic pure bending with variable amplitudes. Priyadarsini et al. (2012) experimentally and analytically examined the buckling of layered composite cylinders subjected to static and dynamic axial compression. Yazdani and Nayebi (2013) studied the damage of thin-walled tubes under cyclic bending with a fixed internal pressure. Shariati et al. (2014) experimentally studied the cyclic-bending response and failure of SS316L cantilevered cylindrical shells. Elchalakani et al. (2016) determined new ductile slenderness limits for CFT structures in the plastic design by employing the measured strain in plastic bending tests. Shamass et al. (2017) investigated the elastoplastic buckling of thin-walled circular tubes that was subjected to a non-proportional loading.

In 1998, Pan et al. began experimentally and theoretically to investigate the response and failure of circular tubes with different curvature ($\dot{\kappa}$) rates or D_o/t ratios submitted to cyclic bending. Pan and Her (1998) experimentally studied the response and collapse of SUS304 stainless steel tubes under cyclic bending at different $\dot{\kappa}$ and discovered that increasing the $\dot{\kappa}$ increased the hardening of tubes. Lee et al. (2001) investigated SUS304 stainless steel tubes with different D_o/t ratios subjected to cyclic bending. Four groups of tubes with different D_o/t ratios were tested, and four parallel straight lines were obtained for the κ_c-N_b relationships on a log-log scale. Later, Pan and Lee (2002) studied the mean curvature effect on the response and buckling of tubes undertaken cyclic bending; this effect was experimentally investigated by employing different curvature ratios (i.e., the minimum curvature divided by the maximum curvature). Chang et al. (2005) explored the cyclic bending response and collapse of 316L stainless steel tubes at different $\dot{\kappa}$; the endochronic theory and the principle of virtual work were employed to describe the moment (M)-curvature (κ) and $\Delta D_o/D_o-\kappa$ relationships. Chang and Pan (2009) conducted experiments on the deterioration and buckling of SUS304 stainless steel tubes with different D_o/t ratios under cyclic bending. This investigation also introduced a new model for

predicting the buckling life.

In 2010, Pan et al. began experimentally and analytically studies the behavior and failure of notched tubes submitted to cyclic bending. Lee et al. (2010) experimentally examined variations of $\Delta D_o/D_o$ for sharp-notched SUS304 stainless steel tubes undertaken cyclic bending. Later, Lee (2010) inspected the response of circular tubes with different notch depths submitted to cyclic bending; this work introduced a new model for predicting N_b . Thereafter, Lee et al. (2013) experimentally investigated the response and collapse of sharp-notched SUS304 stainless steel tubes under cyclic bending at three different $\dot{\kappa}$; correlations between notch depth and $\dot{\kappa}$ were also included in their study. Lee et al. (2014) explored the pure bending creep and pure bending relaxation responses of sharp-notched SUS304 stainless steel tubes. The Bailey-Norton law was modified to describe the creep curvature-time and relaxation moment-time relationships. Chung et al. (2016) inspected the response and buckling of sharp-notched 6061-T6 aluminum alloy tubes submitted to cyclic bending. The κ_c-N_b relationship displayed significant differences from that observed in sharp-notched SUS304 stainless steel tubes under cyclic bending (Lee et al. (2013)). However, all studies of the notch shape were the circumferential sharp notch as shown in Fig. 1(a).

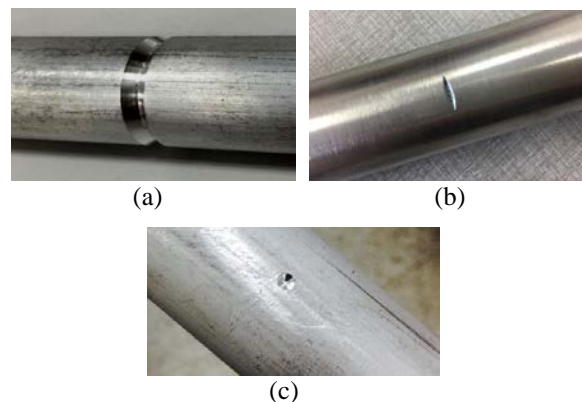


Fig. 1. (a) A picture of the circumferential sharp-notched tube, (b) a picture of the local sharp-cut tube, and (c) a picture of the local sharp-grooved tube.

Later, Lee et al. (2016) examined the behavior of local sharp-notched 6061-T6 aluminum alloy tubes submitted to cyclic bending. The type of the local sharp notch was a local sharp cut as shown in Fig. 1(b). In addition, the $M-\kappa$ and $\Delta D_o/D_o-\kappa$ relationships were analyzed by using ANSYS. Thereafter, Lee et al. (2018) explored the response and failure of local sharp-notched SUS304 stainless steel tubes undertaken cyclic bending. The type of the local sharp notch was a local sharp groove as shown in Fig. 1(c). The $M-\kappa$ relationships were similar to that tested by Lee et al. (2016), however, the $\Delta D_o/D_o-\kappa$

relationships were quite different. In addition, the $M-\kappa$ and $\Delta D_o/D_o-\kappa$ relationships were also analyzed by using ANSYS.

In the present study, round-hole 6061-T6 aluminum alloy tubes with different hole diameters and hole directions subjected to cyclic bending were experimentally investigated. A tube-bending machine and curvature-ovalization measurement apparatus were employed to conduct curvature-controlled cyclic bending tests. The quantities of M , κ and $\Delta D_o/D_o$ were measured by the testing devices. Additionally, the number of bending cycles required to ignite failure (N_f) was also recorded. For theoretical analysis, the finite-element software ANSYS was employed to simulate the $M-\kappa$ and $\Delta D_o/D_o-\kappa$ relationships. In addition, an empirical formula was proposed for simulating the κ_c-N_f relationship

EXPERIMENTS

The tube-bending machine and the curvature-ovalization measurement apparatus were employed to conduct curvature-controlled cyclic bending tests on round-hole 6061-T6 aluminum alloy tubes with different hole diameters and hole directions. The bending device, measurement apparatus, materials, specimens, and test procedures are stated below.

Experimental Device

Fig. 2(a) schematically displays the experiment performed by a specially constructed tube-bending machine. This device was built to conduct cyclic bending tests. Details of the experimental device can be found in numerous papers (e.g., Pan and Her (1998), Lee et al. (2001), Pan and Lee (2002), Chang et al. (2005)). Fig. 2(b) schematically exhibits a light-weight equipment to control and measure the κ and $\Delta D_o/D_o$ of the tube designed by Pan et al. (1998). In this equipment, two side-inclinometers are used to detect the angle changes of tubes during cyclic bending. A simple calculation can be employed to determine the κ according to angle changes. Details of the equipment and calculation can be found in the study by Pan et al. (1998). In addition, the magnetic detector and block in the central portion of the equipment were employed to measure the $\Delta D_o/D_o$.

Material and Specimens

6061-T6 aluminum alloy tubes were adopted for the cyclic bending tests. The tubes' chemical composition (weight %) is Mg (0.937), Si (0.535), Fe (0.139), Zn (0.098), Mn (0.022), Cr (0.022), ..., and a few other trace elements, with the remainder being Al. The 0.2% strain offset yield stress (σ_0) is 285

MPa, the ultimate tensile stress (σ_u) is 320 MPa and the percent elongation ($100\epsilon_t$) is 23 %.

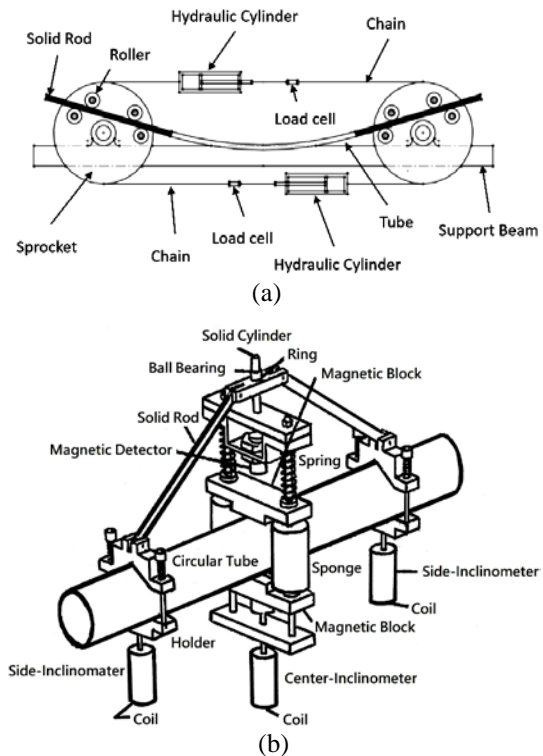


Fig. 2. (a) A schematic drawing of the bending device, and (b) a schematic drawing of the curvature-ovalization measurement apparatus.

The original tubes with $D_o = 35.0$ mm and $t = 3.0$ mm were drilled to obtain the expected holes. In this study, five hole diameters (d) were considered: 2, 4, 6, 8, and 10 mm. Fig. 3 shows a picture of round-hole tubes with $d = 2, 4, 6, 8$ and 10 mm. Because the hole is localized, the hole direction (ϕ) may also affect the response and failure of tubes. Therefore, ϕ must be considered. Fig. 4 demonstrates that ϕ of $0^\circ, 30^\circ, 60^\circ, 90^\circ, 120^\circ, 150^\circ,$ and 180° were considered. Since the cyclic bending moment was in z direction, the same response was presented for $\phi = 0^\circ$ and $180^\circ, 30^\circ$ and $150^\circ,$ and 60° and 120° . Therefore, only four $\phi, 0^\circ, 30^\circ, 60^\circ,$ and $90^\circ,$ were considered in this investigation. In addition, the κ_c was normalized using $\kappa_o = t/D_o^2$ (Kyriakides and Shaw (1987)).

Test Procedures

The cyclic bending tests were performed under curvature control with a curvature rate of $0.03 \text{ m}^{-1}\text{s}^{-1}$. The M was measured by two load cells settled in the tube-bending machine (Fig. 2(a)). The κ and $\Delta D_o/D_o$ were measured by the equipment in Fig. 2(b). Simultaneously, the N_f was also recorded.



Fig. 3. A picture of round-hole 6061-T6 aluminum alloy tubes with different d .

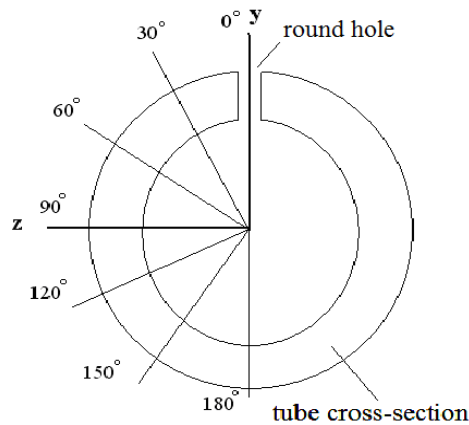


Fig. 4. A schematic drawing of the tube cross-section with a round hole at different ϕ .

FINITE ELEMENT ANSYS ANALYSIS

In this study, the experimental mechanical behavior of round-hole 6061-T6 aluminum alloy tubes subjected to cyclic bending presented the $M-\kappa$ and $\Delta D_o/D_o-\kappa$ relationships. Finite element software “ANSYS” was used to analyze the aforementioned mechanical behavior. The uniaxial stress-strain curves, elements, model, mesh, boundary conditions, and loading conditions are stated below.

Uniaxial Stress-strain Curves

Fig. 5 shows the tested and ANSYS-constructed uniaxial stress (σ) - strain (ϵ) curves for the 6061-T6 aluminum alloy. The kinematic hardening rule was used as the hardening rule for reverse and subsequent cyclic loading.

ANSYS Element and Model

Due to the 3D geometry and elastioplastic deformation of the tube, the SOLID 185 element built in ANSYS was employed for the analysis. This element is a tetrahedral element which is suitable for analyzing tubes subjected to bending. Due to the

right-left symmetry of tubes, only half of the tube model was constructed. Fig. 6 shows the mesh for half of round-hole tube constructed by ANSYS.

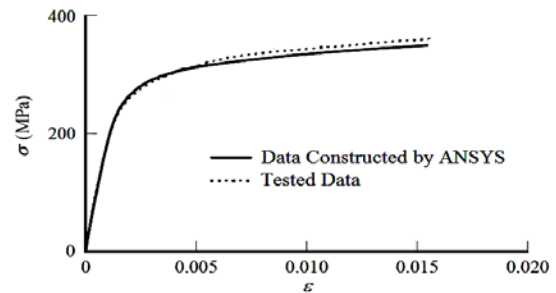
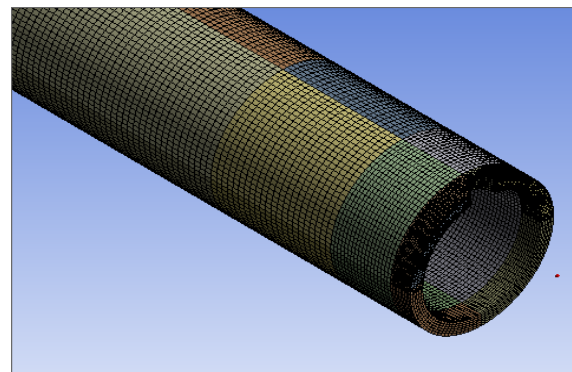
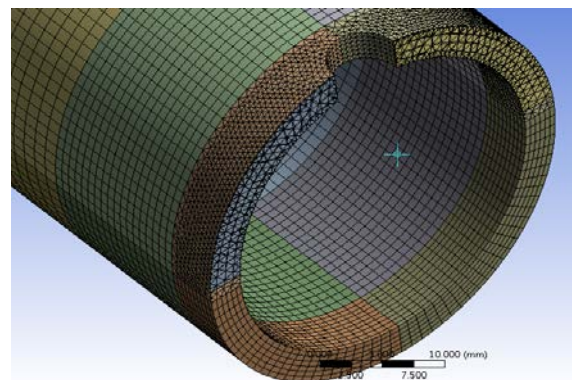


Fig. 5. Tested and ANSYS constructed data of the uniaxial stress (σ) - strain (ϵ) curve for 6061-T6 aluminum alloy.



(a)



(b)

Fig. 6. (a) Mesh constructed by ANSYS for the half tube, (b) magnified view around the round hole.

Boundary and Loading Conditions

Fig. 7 shows the restrictions on the plane of the central cross-section for a tube under cyclic bending. Note that the plane of the central cross-section is a symmetrical plane. Because the bending moment was in the z -direction only, the frictionless roller support was fixed to the plane of the central cross-section, and the displacement in the z -direction of this plane was set to zero. Fig. 8 demonstrates the loading conditions constructed by ANSYS. According to the

movement of the tube-bending machine, the rotation could move freely in the z -direction, thus, the remote displacement in the z -direction was set to be unrestricted. In addition, because the bending moment was only in the z -direction, thus, the rotations in the x - and y -directions were put to zero.

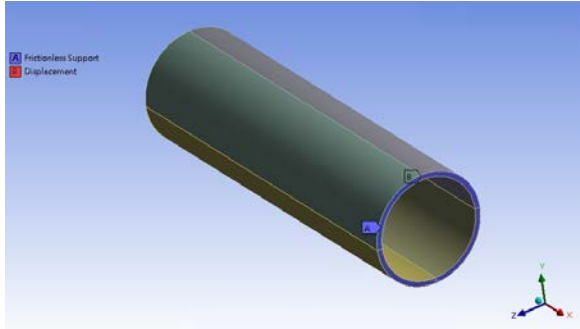


Fig. 7. Restrictions on the plane of the central cross section constructed by ANSYS.

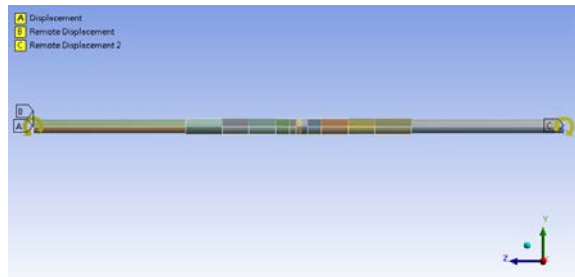


Fig. 8. Loading conditions constructed by ANSYS.

Since the tests were curvature-controlled cyclic bending, the rotation angle θ was employed as the input data in this study (Fig. 9). The relationship between θ and κ was derived to be:

$$\kappa = 1 / \rho = 2\theta / L_0, \quad (1)$$

where ρ is the radius of the curvature, and L_0 is the original tube length

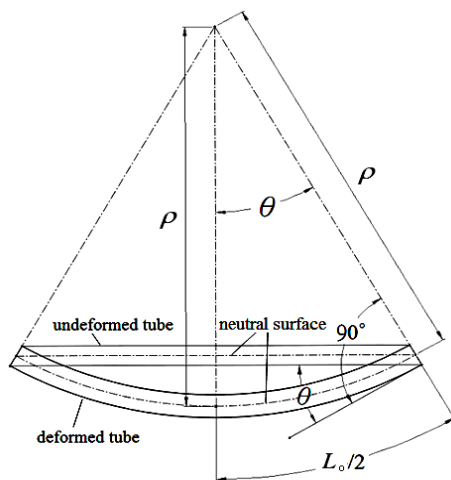
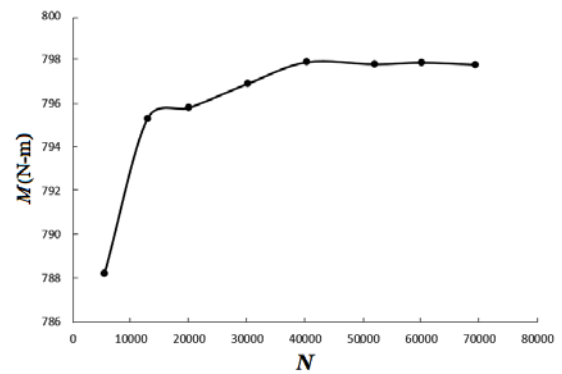


Fig. 9. Relationship between θ and κ for a tube under pure bending.

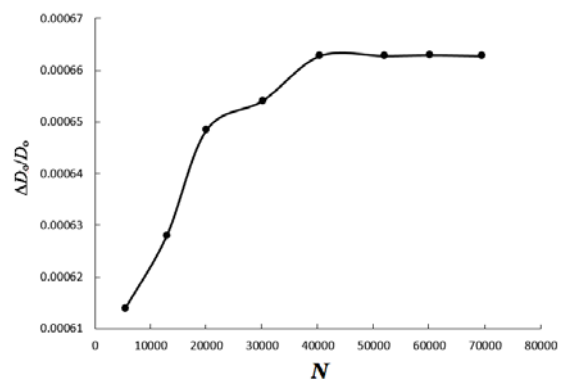
Convergent Analysis

The fineness of the mesh segmentation is closely related to the convergence of the simulation and the accuracy of the results. The finer the mesh, the more accurate the results, but the more operations are performed during the simulation, and the longer it takes. Therefore, in order to make a reasonable balance between the accuracy and the calculation time, the convergence analysis of the number of meshes is performed before solving.

Figs. 10 (a) and 10(b) respectively show the ANSYS determined M -number of grids (N) and $\Delta D_o/D_o$ - N relationships for round-hole 6061-T6 aluminum alloy tubes with $d = 2$ mm and $\phi = 0^\circ$ under cyclic bending. The magnitudes of M and $\Delta D_o/D_o$ are determined at $\kappa = 0.4 \text{ m}^{-1}$. It can be seen that M increases as N increases, until N is 40000, which tends to be stable. Simultaneously, $\Delta D_o/D_o$ also increases as N increases, until N is 40000, which also tends to be stable. Therefore, the number of the grids is selected to be 40000 in this study.



(a)



(b)

Fig. 10. (a) Convergent analysis of the M - N relationship, and (b) convergent analysis of the $\Delta D_o/D_o$ - N relationship.

EXPERIMENTAL RESULTS, SIMULATED RESULTS AND DISCUSSION

Response of Round-hole 6061-T6 Aluminum Alloy Tubes under Cyclic Bending

Fig. 11(a) depicts a typical set of experimental cyclic $M-\kappa$ curve for round-hole 6061-T6 aluminum alloy tube with $d = 6$ mm and $\phi = 0^\circ$ when subjected to cyclic bending. The tube shows stable $M-\kappa$ response from the first bending cycle. Because the holes are small and localized, the $M-\kappa$ curves for different d and ϕ are nearly identical. Therefore, the $M-\kappa$ curves for different d and ϕ are not shown in this paper. Fig. 11(b) shows the ANSYS-simulated $M-\kappa$ curve for Fig. 11(a).

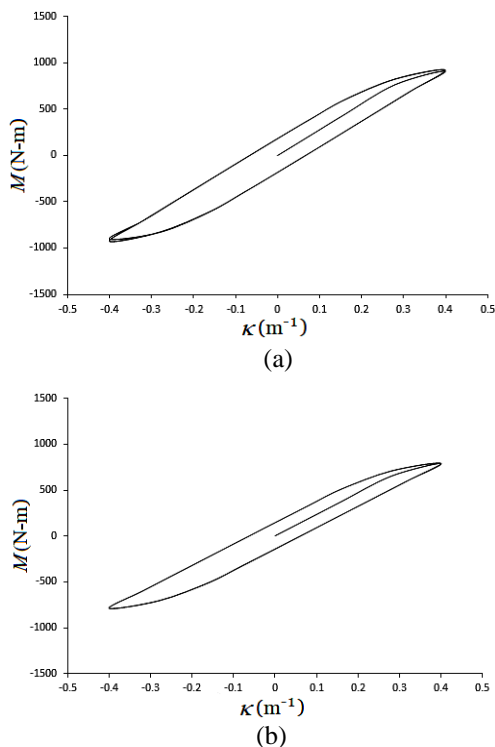


Fig. 11. (a) Experimental and (b) ANSYS-simulated $M-\kappa$ curves for round-hole 6061-T6 aluminum alloy tubes with $\phi = 0^\circ$ and $d = 6$ mm under cyclic bending.

Figs. 12(a)-12(e) respectively demonstrate the experimental $\Delta D_o/D_o-\kappa$ relationships for round-hole 6061-T6 aluminum alloy tubes with $\phi = 0^\circ$ and $d = 2, 4, 6, 8,$ and 10 mm subjected to cyclic bending. The $\Delta D_o/D_o-\kappa$ relationships show ratcheting and increasing trend with the number of bending cycles. The $\Delta D_o/D_o-\kappa$ curve is symmetrical for a smaller d . However, a larger d in the round-hole tube causes a larger $\Delta D_o/D_o$. Moreover, a larger d leads to a more asymmetrical appearance of the $\Delta D_o/D_o-\kappa$ relationship. The $\Delta D_o/D_o-\kappa$ relationships are asymmetrical bow shape which is different from that of sharp-notched SUS304 stainless steel tubes tested by Lee (2010), Lee et al. (2013) and Lee et al. (2018), and that of sharp-notched 6061-T6 aluminum alloy tubes tested by Chung et al. (2016) and Lee et al.

(2016). In addition, $\Delta D_o/D_o$ continues to increase when the round hole is under tension. However, $\Delta D_o/D_o$ continues to decrease when the round hole is under compression. Figs. 13(a)-13(e) respectively illustrate the corresponding ANSYS-simulated $\Delta D_o/D_o-\kappa$ relationships for Figs. 12(a)-12(e)

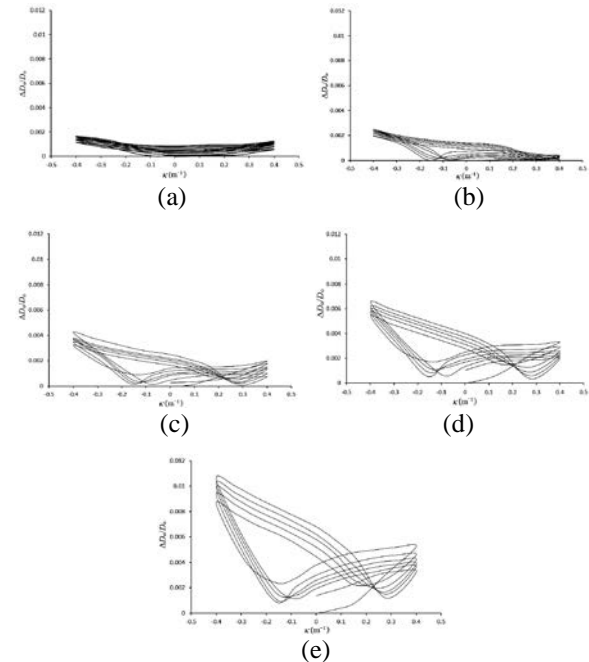


Fig. 12. Experimental $\Delta D_o/D_o-\kappa$ curves for round-hole 6061-T6 aluminum alloy tubes with $\phi = 0^\circ$ and $d =$ (a) 2, (b) 4, (c) 6, (d) 8, and (e) 10 mm under cyclic bending.

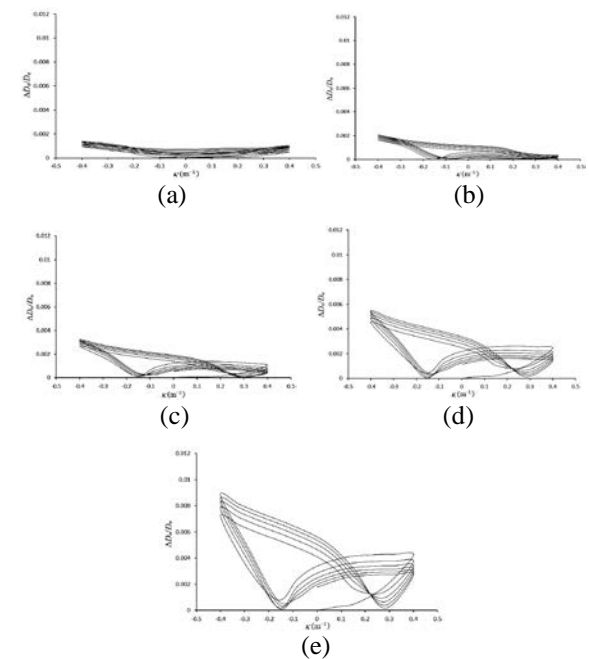


Fig. 13. ANSYS-simulated $\Delta D_o/D_o-\kappa$ curves for round-hole 6061-T6 aluminum alloy tubes with $\phi = 0^\circ$ and $d =$ (a) 2, (b) 4, (c) 6, (d) 8, and (e) 10 mm under cyclic bending.

Figs. 14(a)-14(d) respectively depict the experimental $\Delta D_o/D_o-\kappa$ relationships for round-hole 6061-T6 aluminum alloy tubes with $d = 10$ mm and $\phi = 0^\circ, 30^\circ, 60^\circ,$ and 90° submitted to cyclic bending. Note that the situation of $d = 10$ mm and $\phi = 0^\circ$ for the round-hole 6061-T6 aluminum alloy tube in Fig. 14(a) is identical to that in Fig. 12(e). It is observed that $\Delta D_o/D_o$ also increases in a ratcheting way as the number of bending cycles increases. A larger ϕ causes a more symmetrical appearance of the $\Delta D_o/D_o-\kappa$ relationship and leads to less $\Delta D_o/D_o$ in the tubes. Because the trends of $\Delta D_o/D_o-\kappa$ curves for other d with $\phi = 0^\circ, 30^\circ, 60^\circ,$ and 90° are similar to those observed in Figs. 14(a)-14(d), the $\Delta D_o/D_o-\kappa$ curves for other d at $\phi = 0^\circ, 30^\circ, 60^\circ,$ and 90° are not shown in this paper. Figs. 15(a)-15(d) respectively demonstrate the corresponding ANSYS-simulated $\Delta D_o/D_o-\kappa$ relationships for Figs. 14(a)-14(d).

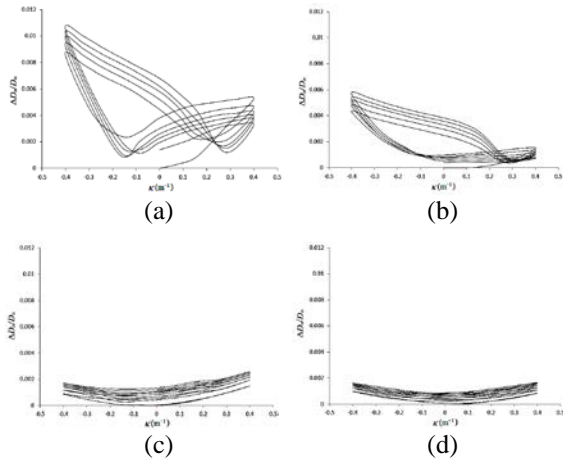


Fig. 14. Experimental $\Delta D_o/D_o-\kappa$ curves for round-hole 6061-T6 aluminum alloy tubes with $d = 10$ mm and $\phi =$ (a) $0^\circ,$ (b) $30^\circ,$ (c) $60^\circ,$ and (d) 90° under cyclic bending.

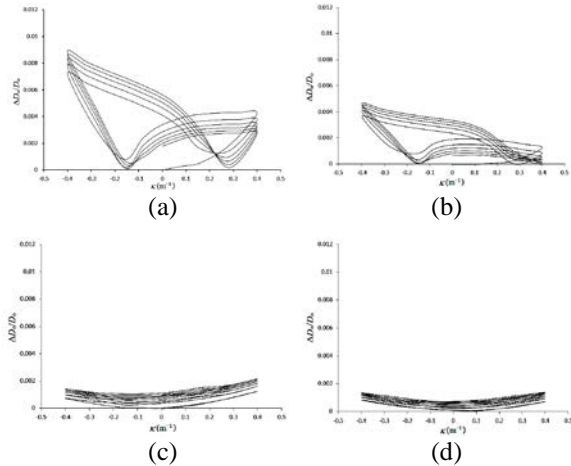


Fig. 15. ANSYS-simulated $\Delta D_o/D_o-\kappa$ curves for round-hole 6061-T6 aluminum alloy tubes with $d = 10$ mm and $\phi =$ (a) $0^\circ,$ (b) $30^\circ,$ (c) $60^\circ,$ and (d) 90° under cyclic bending.

Failure of Round-hole 6061-T6 Aluminum Alloy Tubes under Cyclic Bending

Figs. 16(a)-16(d) respectively show the experimental data of κ_c/κ_o-N_f relationships for round-hole 6061-T6 aluminum alloy tubes with different d and $\phi = 0^\circ, 30^\circ, 60^\circ,$ and 90° subjected to cyclic bending. Figs. 17(a)-17(d) respectively present the experimental data in Figs. 16(a)-16(d) plotted on a log-log scale in dot lines. These straight dotted lines were determined by the least-squares method. It can be seen that for a certain $\phi,$ five almost-parallel lines correspond to five different d for the κ_c/κ_o-N_f relationships on a log-log scale. However, the slopes of parallel lines for four different ϕ are different.

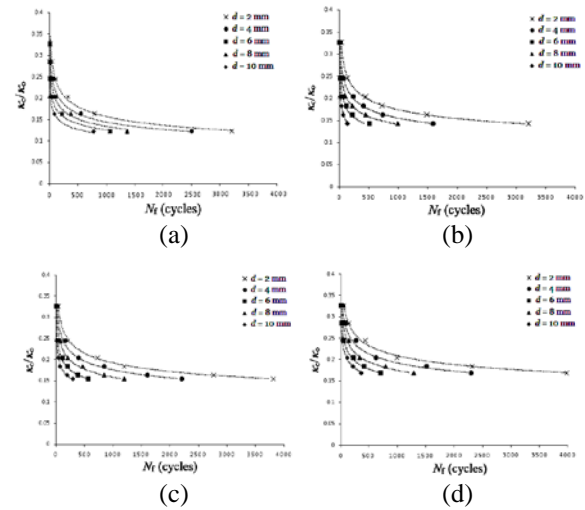


Fig. 16. Experimental κ_c/κ_o-N_f relationships for round-hole 6061-T6 aluminum alloy tubes with different d and $\phi =$ (a) $0^\circ,$ (b) $30^\circ,$ (c) $60^\circ,$ and (d) 90° under cyclic bending.

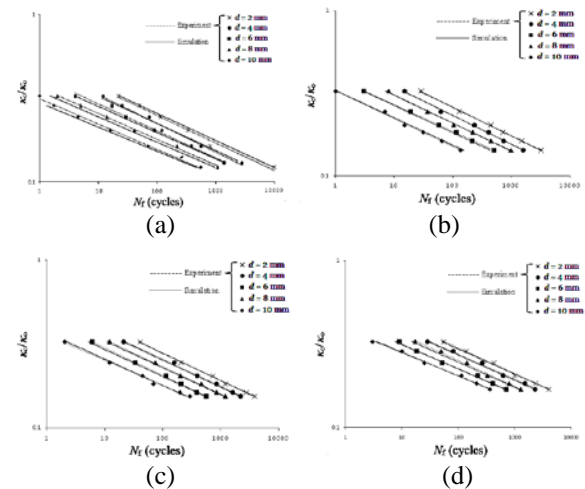


Fig. 17. Experimental and simulated κ_c/κ_o-N_f relationships for round-hole 6061-T6 aluminum alloy tubes with different d and $\phi =$ (a) $0^\circ,$ (b) $30^\circ,$ (c) $60^\circ,$ and (d) 90° under cyclic bending on a log-log scale.

The empirical formula proposed by Kyriakides and Shaw (1987) for the relationship between κ_c/κ_0 and N_f was employed in this paper to be:

$$\kappa_c/\kappa_0 = C(N_f)^{-\alpha} \quad \text{or} \quad \log \kappa_c/\kappa_0 = \log C - \alpha \log N_f, \quad (2a, b)$$

where C and α are material parameters. The magnitude of C is equal to κ_c/κ_0 when $N_f = 1$ and α is the slope of the log-log plot. According to the experimental data in Figs. 17(a)-17(d), the values of C for every d at different ϕ can be obtained as shown in Table 1. The experimental $\log C$ - d/t relationship for different ϕ is demonstrated in Fig. 18(a). The straight dotted lines corresponding to $\phi = 0^\circ, 30^\circ, 60^\circ,$ and 90° in the figure were determined by the least-squares method. The dotted lines nearly intersect at the coordinates of $(0, 0.643)$ as shown in Fig. 18(a). It means that C is the same for every ϕ when d is equal to 0 mm (i.e., a smooth tube). In this study, an empirical formula was proposed as follows:

$$\log C = -m\left(\frac{d}{t}\right) + b, \quad (3)$$

where m and b are material parameters. From Fig. 18(a), b was determined to be 0.643 for $d/t = 0.0$ and the values of m were respectively determined to be 1.37, 1.09, 1.00, and 0.94 for $\phi = 0^\circ, 30^\circ, 60^\circ,$ and 90° . The m - ϕ relationship is shown in Fig. 18(b), and a formula of this relationship can be written as follows:

$$m = a_1\phi + a_2 \quad 0 \leq \phi \leq \pi/2, \quad (4)$$

where a_1 and a_2 are material parameters which were respectively determined by curve fitting to be 2.56 and 0.073. In Fig. 18(a), the solid lines are the the simulated $\log C$ - a/t relationships for four different ϕ .

According to the experimental data in Figs. 17(a)-17(d), the values of α for $\phi = 0^\circ, 30^\circ, 60^\circ,$ and 90° can be determined in Table 2. The linear relationship of $\alpha^{1/3}$ and ϕ is demonstrated in Fig. 19, and a formula of this relationship can be proposed as follow:

$$\alpha^{1/3} = b_1\phi + b_2 \quad 0 \leq \phi \leq \pi/2, \quad (5)$$

In which b_1 and b_2 are material parameters that can be respectively determined by curve fitting to be -0.046 and 0.88. Figs. 17(a)-17(d) respectively depict the simulated κ_c/κ_0 - N_f relationships for round-hole 6061-T6 aluminum alloy tubes with different d and $\phi = 0^\circ, 30^\circ, 60^\circ,$ and 90° on a log-log scale in solid lines. In addition, Fig. 20 demonstrates the failure of round-hole 6061-T6 aluminum alloy tubes subjected to cyclic bending. It can be seen that cracks initiate at

the round hole and once the crack is visible the tubes breaks rapidly.

Table 1. Experimental magnitudes of $\log C$ for every d at different ϕ .

	$d = 2$ mm	$d = 4$ mm	$d = 6$ mm	$d = 8$ mm	$d = 10$ mm
$\phi = 0^\circ$	0.585	0.502	0.436	0.366	0.316
$\phi = 30^\circ$	0.592	0.509	0.453	0.401	0.345
$\phi = 60^\circ$	0.581	0.542	0.469	0.421	0.375
$\phi = 90^\circ$	0.601	0.549	0.489	0.449	0.398

Table 2. Experimental magnitudes of α at different ϕ .

ϕ	0°	30°	60°	90°
α	0.177	0.169	0.160	0.148

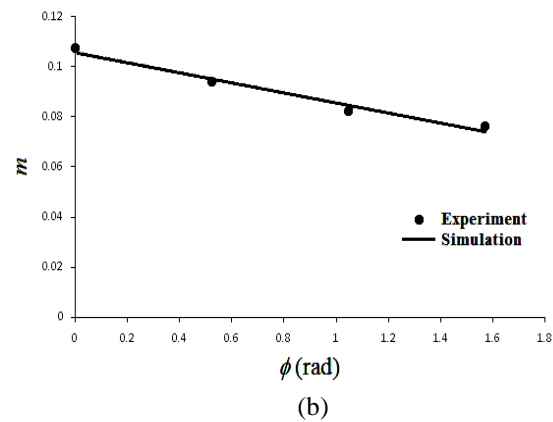
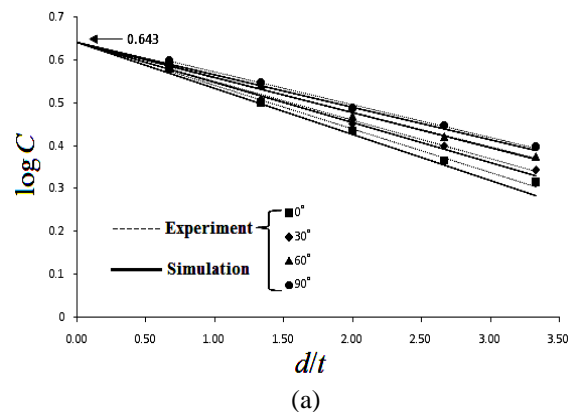


Fig. 18. Experimental and simulated (a) relationship between $\log C$ and d/t for different ϕ , and (b) relationship between m and ϕ .

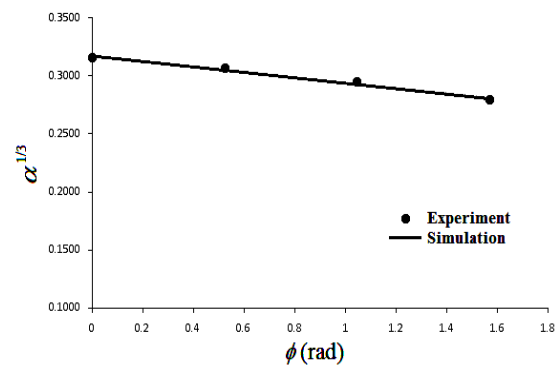


Fig. 19. Relationship between $\alpha^{1/3}$ and ϕ .

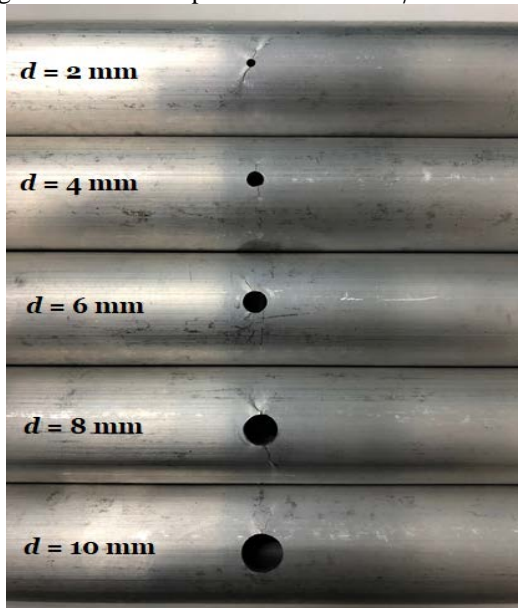


Fig. 20. A picture of the failure for round-hole 6061-T6 aluminum alloy tubes submitted to cyclic bending.

CONCLUSIONS

This study investigated the response and failure of round-hole 6061-T6 aluminum alloy circular tubes with different d and ϕ subjected to cyclic bending. According to the experimental and theoretical results, the following conclusions were drawn:

- (1) The experimental M - κ relationship for round-hole 6061-T6 aluminum alloy tubes with any d and ϕ exhibits a closed and stable hysteresis loop. The M values are almost equal to each other at the maximum and minimum controlled curvatures. Because the holes are small and localized, the M - κ curves for different d and ϕ are nearly identical.
- (2) The experimental $\Delta D_o/D_o$ - κ relationship for round-hole 6061-T6 aluminum alloy tubes with any d exhibits an increase and ratcheting with an increase in the number of bending cycles. The $\Delta D_o/D_o$ - κ relationships show asymmetrical bow shapes. A larger d leads to a more asymmetry $\Delta D_o/D_o$ - κ relationship and larger $\Delta D_o/D_o$. In addition, a larger ϕ causes a more symmetrical $\Delta D_o/D_o$ - κ relationship and smaller $\Delta D_o/D_o$.
- (3) By employing the proper uniaxial stress-strain relationship, model, mesh, boundary conditions, and loading conditions, the finite element ANSYS was used to simulate the behavior of round-hole circular tubes subjected to cyclic bending. By employing the convergent analysis, the number of the grids was selected to be 40000 in this study. The experimental M - κ and $\Delta D_o/D_o$ - κ relationships

were compared with the ANSYS simulation. Good agreement between the experimental and simulated results was achieved.

- (4) The empirical formulation of Eq. (2) introduced by Kyriakides and Shaw (1987) was modified so that it could be used to simulate the κ/κ_o - N_f relationship for round-hole 6061-T6 aluminum alloy tubes with different d and ϕ subjected to cyclic bending. According to the experimental data, the formulations for describing C were proposed in Eqs. (3) and (4), and the formulation for describing α was proposed in Eq. (5). It was observed that the simulated results were in good agreement with the experimental data, as shown in Figs. 17(a)-17(d).

ACKNOWLEDGEMENT

The research was executed with the support of the Ministry of Science and Technology under grant MOST 106-2221-E-006-097. We sincerely thank them for their assistance.

REFERENCES

- Bechle, N.J., and Kyriakides, S., "Localization of NiTi Tubes under Bending,"; *Int. J. Solids Struct.*, Vol. 51, No. 5, pp. 967-980 (2014).
- Chang, K.H., and Pan, W.F., "Buckling Life Estimation of Circular Tubes under Cyclic Bending,"; *Int. J. Solids Struct.*, Vol. 46, No. 2, pp. 254-270 (2009).
- Chang, K.H., Hsu, C.M., Sheu, S.R., and Pan, W.F., "Viscoplastic Response and Collapse of 316L Stainless Steel Tubes under Cyclic Bending,"; *Steel Comp. Struct.*, Vol. 5, No. 5, pp. 359-374 (2005).
- Chung, C.C., Lee, K.L., and Pan, W.F., "Collapse of Sharp-notched 6061-T6 Aluminum Alloy Tubes under Cyclic Bending,"; *Int. J. Struct. Stab. Dyn.*, Vol. 26, No. 7, 1550035 [24 pages] (2016).
- Corona, E., and Kyriakides, S., "An Experimental Investigation of the Degradation and Buckling of Circular Tubes under Cyclic Bending and External Pressure,"; *Thin-Walled Struct.*, Vol. 12, No. 3, pp. 229-263 (1991).
- Corona, E., and Kyriakides, S., "Asymmetric Collapse Modes of Pipes under Combined Bending and Pressure,"; *Int. J. Solids Struct.*, Vol. 24, No. 5, pp. 505-535 (2000).
- Corona, E., Lee, L.H., and Kyriakides, S., "Yield Anisotropic Effects on Buckling of Circular Tubes under Bending,"; *Int. J. Solids Struct.*, Vol. 43, No. 22, pp. 7099-7118 (2006).
- Corradi, L., Luzzi, L. and Trudi, F., "Plasticity-

- instability Coupling Effects on the Collapse of Thick Tubes,”; *Int. J. Struct. Stab. Dyn.*, Vol. 5, No. 1, pp. 1-18 (2005).
- Elchalakani, M., Karrech, A., Hassanein, M.F., and Yang, B., “Plastic and Yield Slenderness Limits for Circular Concrete Filled Tubes Subjected to Static Pure Bending,”; *Thin-Walled Struct.*, Vol. 109, pp. 50-64 (2016).
- Elchalakani, M., and Zhao X.L., “Concrete-Filled Cold-formed Circular Steel Tubes Subjected to Variable Amplitude Cyclic Pure Bending,”; *Eng. Struct.*, Vol. 30, No. 2, pp. 287-299 (2008).
- Elchalakani, M., Zhao, X.L., and Grzebieta, R.H., “Plastic Mechanism Analysis of Circular Tubes under Pure Bending,”; *Int. J. Mech. Sci.*, Vol. 44, No. 6, pp. 1117-1143 (2002).
- Elchalakani, M., Zhao, X.L., and Grzebieta, R.H., “Variable Amplitude Cyclic Pure Bending Tests to Determine Fully Ductile Section Slenderness Limits for Cold-formed CHS,”; *Eng. Struct.*, Vol. 28, No. 9, pp. 1223-1235 (2006)
- Jiang, D., Kyriakides, S., Bechle, N.J., and Landis, C.M., “Bending of Pseudoelastic NiTi Tubes,”; *Int. J. Solids Struct.*, Vol. 124, pp. 192-214 (2017)
- Jiao, H., and Zhao, X.L., “Section Slenderness Limits of Very High Strength Circular Steel Tubes in Bending,”; *Thin-Walled Struct.*, Vol. 42, No. 9, pp. 1257-1271 (2004).
- Kyriakides, S., and Shaw, P.K., “Inelastic Buckling of Tubes under Cyclic Loads,”; *ASME J. Press. Ves. Tech.*, Vol. 109, No. 2, pp. 169-178 (1987).
- Lee, K.L., “Mechanical Behavior and Buckling Failure of Sharp-notched Circular Tubes under Cyclic Bending,”; *Struct. Eng. Mech.*, Vol. 34, No. 3, pp. 367-376 (2010).
- Lee, K.L., Chang, K.H., and Pan, W.F., “Failure Life Estimation of Sharp-notched Circular Tubes with Different Notch Depths under Cyclic Bending,”; *Struct. Eng. Mech.*, Vol. 60, No. 3, pp. 387-404 (2016).
- Lee, K.L., Chang, K.H., and Pan, W.F., “Effects of Notch Depth and Direction on Stability of Local Sharp-notched Circular Tubes Subjected to Cyclic Bending,”; *Int. J. Struct. Stab. Dyn.*, Vol. 18, No. 7, 1850099 [23 pages] (2018).
- Lee, K.L., Hsu, C.M., and Pan, W.F., “Viscoplastic Collapse of Sharp-notched Circular Tubes under Cyclic Bending,”; *Acta Mech. Solida Sinica*, Vol. 26, No. 6, pp. 629-641 (2013).
- Lee, K.L., Hsu, C.M., and Pan, W.F., “Response of Sharp-notched Circular Tubes under Bending Creep and Relaxation,”; *Mech. Eng. J.*, Vol. 1, No. 2, pp. 1-14 (2014).
- Lee, K.L., Hung, C.Y., and Pan, W.F., “Variation of Ovalization for Sharp-notched Circular Tubes under Cyclic Bending,”; *J. Mech.*, Vol. 26, No. 3, pp. 403-411 (2010).
- Lee, K.L., Pan, W.F., and Kuo, J.N., “The Influence of the Diameter-to-thickness Ratio on the Stability of Circular Tubes under Cyclic Bending,”; *Int. J. Solids Struct.*, Vol. 38, No. 14, pp. 2401-2413 (2001).
- Limam, A., Lee, L.H., and Kyriakides, S., “On the Collapse of Dented Tubes under Combined Bending and Internal Pressure,”; *Int. J. Solids Struct.*, Vol. 55, No. 1, pp. 1-12 (2012).
- Limam, A., Lee, L.H., Corona, E., and Kyriakides, S., “Inelastic Wrinkling and Collapse of Tubes under Combined Bending and Internal Pressure,”; *Int. J. Mech. Sci.*, Vol. 52, No. 5, pp. 37-47 (2010).
- Pan, W.F., and Her, Y.S., “Viscoplastic Collapse of Thin-walled Tubes under Cyclic Bending,”; *ASME J. Eng. Mat. Tech.*, Vol. 120, No. 4, pp. 287-290 (1998).
- Pan, W.F., and Lee, K.L., “The Effect of Mean Curvature on the Response and Collapse of Thin-walled Tubes under Cyclic Bending,”; *JSME Int. J., Ser. A*, Vol. 28, No. 2, pp. 495-514 (2002).
- Pan, W.F., Wang, T.R., and Hsu, C.M., “A Curvature-ovalization Measurement Apparatus for Circular Tubes under Cyclic Bending,”; *Exp. Mech.*, Vol. 38, No. 2, pp. 99-102 (1998).
- Priyadarsini, R.S., Kalyanaraman, V., and Srinivasan, S.M., “Numerical and Experimental Study of Buckling of Advanced Fiber Composite Cylinders under Axial Compression,”; *Int. J. Struct. Stab. Dyn.*, Vol. 12, No. 4, 1250028 [25 pages] (2012).
- Shamass, R., Alfano, G., and Guarracino, F., “On Elastoplastic Buckling Analysis of Cylinders under Nonproportional Loading by Differential Quadrature Method,”; *Int. J. Struct. Stab. Dyn.*, Vol. 17, No. 7, 1750072 [40 pages] (2017).
- Shariati, M., Kolasangiani, K., Norouzi, G., and Shahnavaaz, A., “Experimental Study of SS316L Cantilevered Cylindrical Shells under Cyclic Bending Load,”; *Thin-Walled Struct.*, Vol. 82, pp. 124-131 (2014).
- Vaze, S., and Corona, E., “Degradation and Collapse of Square Tubes under Cyclic Bending,”; *Thin-Walled Struct.*, Vol. 31, No. 4, pp. 325-341 (1998).
- Yazdani, H., and Nayebi, A., “Continuum Damage Mechanics Analysis of Thin-walled Tube under Cyclic Bending and Internal Constant Pressure,”; *Int. J. Appl. Mech.*, Vol. 5, No. 4, 1350038 [20 pages] (2013).
- Yuan, W., and Mirmiran, A., “Buckling Analysis of Concrete-filled FRP Tubes,”; *Int. J. Struct. Stab. Dyn.*, Vol. 1, No. 3, pp. 367-383 (2001).

NOMENCLATURE

a_1 material parameter

a_2	material parameter
b_1	material parameter
b_2	material parameter
C	material parameter
D_o	original outer diameter
d	hole diameter
L_o	original tube length
M	moment
m	material parameter
N_b	number of bending cycles required to ignite buckling
N_f	number of bending cycles required to ignite failure
t	wall-thickness
α	material parameter
ΔD_o	change in outer diameter
ε	uniaxial strain
κ	curvature
κ_c	cyclic controlled curvature
κ_o	curvature for normalization
θ	half of the central angle
ρ	radius of curvature
σ	uniaxial stress

循環彎曲負載下圓孔管失效之研究

李國龍

遠東科技大學創新設計與創業管理系

翁慕理 潘文峰

國立成功大學工程科學系

摘要

本文主要是實驗與理論研究不同圓孔直徑與圓孔方向的 6061-T6 鋁合金圓孔管在循環彎曲負載下的響應及失效。我們發現，從第一個彎曲循環圈數開始，彎矩-曲率關係即呈現一個幾乎穩定且閉合的遲滯迴圈，圓孔的直徑和方向對迴圈的形狀幾乎沒有影響。然而，隨著循環圈數的增加，橢圓化-曲率關係卻呈現非對稱、棘齒與蝴蝶結狀的成長，且圓孔的直徑和方向對該關係有很大的影響。最後，本研究使用有限元素軟體 ANSYS 來描述彎矩-曲率及橢圓化-曲率的關係，且本研究也提出一個理論模式來描述控制曲率-循環至失效圈數的關係。在與實驗結果比較後發現，理論能夠合理的描述實驗結果。